Nuclear Inst. and Methods in Physics Research, A 944 (2019) 162574

Contents lists available at ScienceDirect

Nuclear Inst. and Methods in Physics Research, A

journal homepage: www.elsevier.com/locate/nima

# Longitudinal response uniformity of a rectangular-shaped plastic scintillator when exposed to mono-energetic gamma-rays

H. Yazdandoust [a], N. Ghal-Eh [b,c,*], M.M. Firoozabadi [a]

[a] Department of Physics, Faculty of Sciences, University of Birjand, P.O. Box 97175-615, Birjand, Iran
[b] School of Physics, Damghan University, P.O. Box 36716-41167, Damghan, Iran
[c] Department of Physics, Faculty of Sciences, Ferdowsi University of Mashhad, P.O. Box 91775-1436, Mashhad, Iran

ARTICLE INFO

*Keywords:*
Plastic scintillator
Non-uniformity
MCNPX-PHOTRACK
FLUKA

ABSTRACT

The longitudinal response uniformity of the rectangular-shaped plastic scintillators used in a thermal neutron imaging system proposed by Ghal-Eh and Green in 2016 is vital for its precise measurements in quality assurance studies of boron neutron capture therapy (BNCT). The MCNPX-PHOTRACK hybrid code has been used to model the response of rectangular plastic scintillator of partially painted surface in order to reduce as much as possible the longitudinal non-uniformity which usually exist in large and/or long scintillators. The results show that the optimum uniformity corresponds to fully-polished surface which coincides with FLUKA light transport simulations.

## 1. Introduction

The radiation detection by organic scintillators is based on the production of light photons as a result of molecular de-excitations following the radiation interactions with scintillator material. Having experienced several attenuations inside the scintillator volume and reflections at the boundaries, the light photons are collected by electronic photosensitive devices, such as a photomultiplier tube (PMT), and they are eventually transformed into electrical pulses. Such a mechanism makes the scintillator response dependent on a number of factors, such as optical characteristics of the scintillator (*e.g.*, attenuation coefficient, refractive index, etc.), presence of different shapes of lightguide as well as the boundary surface types (*i.e.*, polished, painted or metalized), and so on. Furthermore, since photons, depending on their production site, travel different paths until they reach the PMT, the scintillator response may also depend on the location of radiation exposure to the detector.

Therefore, in addition to incident particle transport one has to carefully take into account the detailed scintillation light transport. This can be undertaken either with dedicated light-transport codes (*e.g.*, PHOTRACK [1] and PHOTON [2]) or the light-transport capabilities of general-purpose codes (*e.g.*, FLUKA [3] and GEANT4 [4]).

Long scintillators are widely used in different applications, from nuclear level gauges [5] to muon detections [6] and nuclear calorimetry measurements [7], where in some cases the longitudinal uniformity is a necessary feature. However, in the present study, as an imaging application of long scintillators, the light transport simulation is undertaken for a $2 \times 2 \times 20$ cm$^3$ rectangular NE102 plastic scintillator, which represents one of seven horizontal scintillators that are supposed to be used in the proposed thermal neutron imaging system. The radiation source is a beam of 2.22 MeV gamma-rays generated through $^{1}$H(n$_{th}$, $\gamma$)$^{2}$H reaction when thermal neutrons interact with hydrogen nuclei in the small water phantom ($14 \times 15 \times 20$ cm$^3$) in pre-treatment BNCT facility. The scintillator response has been simulated as follows. The incident radiation energies deposited at different locations inside the scintillator volume have been calculated with the PTRAC card of the MCNPX code (Version 2.6.0, with ENDF/B-VII cross section library) [8], before using the rectangular version of light transport code, PHOTRACK, to calculate the scintillator response. This PHOTRACK code version has been improved by precise wall effect incorporation and then verified. Since the transmissions of light photons in the detector volume eliminates the response uniformity at different longitudinal gamma-ray exposure locations, it has been decided to use the well-known paint removal technique [9] to minimize the response non-uniformity along the scintillator length. Moreover, the light transport capability of FLUKA code has been used to compare with the MCNPX-PHOTRACK results.

## 2. Materials and methods

### 2.1. Thermal neutron imaging system

The development of a reliable and real-time measurement tool for thermal neutron flux mapping inside a water phantom is an extremely important issue in clinical applications of BNCT within the framework

* Corresponding author at: School of Physics, Damghan University, P.O. Box 36716-41167, Damghan, Iran.
*E-mail address:* ghal-eh@du.ac.ir (N. Ghal-Eh).

https://doi.org/10.1016/j.nima.2019.162574
Received 11 June 2019; Received in revised form 16 July 2019; Accepted 11 August 2019
Available online 16 August 2019
0168-9002/

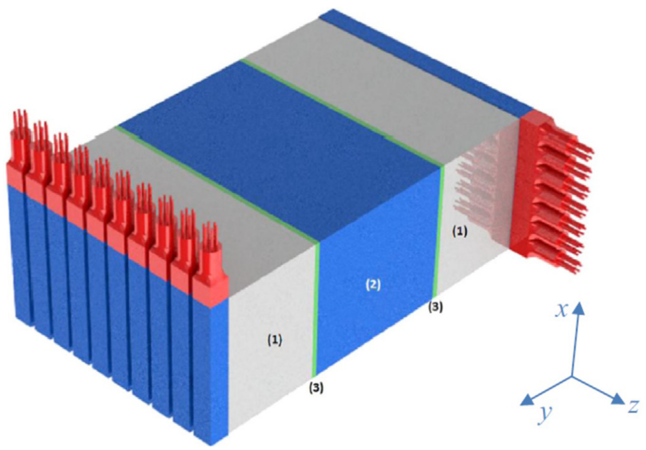


**Fig. 1.** The detection system consists of seven horizontal and ten vertical scintillators, thick lead collimator blocks (1), rectangular water phantom (2), thin cadmium sheets (3) and seventeen PMTs [10].

of pre-treatment quality assurance. In 2016, the conceptual design of an instrument consisting of 17 commercial NE102 plastic scintillators and PMTs together with some shielding/collimator materials of special geometry was proposed [10] as illustrated in Fig. 1. Although the preliminary thermal neutron flux image constructed using the responses of the proposed detection system satisfactorily coincided with the MCNPX neutron flux data, a set of modifications have to be undertaken in order to provide a practical prototype. One of the most important modifications is to include the light transport inside the rectangular scintillators of the detection system which was ignored in previously published simulations.

The incorporation of light transport is necessary to undertake especially in large-sized scintillators as an important step forward in modeling what actually occurs in reality. The size of large scintillators causes most optical photons to undergo considerable light attenuation and numerous reflections at the boundaries before reaching the PMT, which results in a wide range of light collection efficiencies for the light generation points.

It is notable that any non-uniformity of the light collection efficiency along the scintillator cell will disturb the 2D thermal neutron image of the proposed system which then requires a complicated calibration procedure to reproduce the correct thermal neutron flux.

On the other hand, some studies show that the surface covering can greatly affect the light collection efficiency [11] where the response uniformity can be improved by removal of the reflective paint near the PMT window and resulting in better energy resolution [9].

### *2.2. MCNPX-PHOTRACK hybrid code*

The simulation of light transport in scintillators using the MCNPX-PHOTRACK hybrid code is basically performed in two stages as it follows. The geometry, materials and source specifications are introduced in the MCNPX input file before using the PTRAC card in which all required event types are filtered and reported in a general and comprehensive output file. In PTRAC output file, the details of every particle history are recorded in an event-by-event phase space. A robust post-processing program is normally required to extract the coordinates of interaction points within the scintillator cell and also the corresponding deposition energies for all histories from output file. Next, both location and energy information are fed into PHOTRACK, where an appropriate number of optical photons, *i.e.*, proportional to the deposited energy, with isotropic directions are generated and then followed through many boundary crossings, surface reflections/transmission and attenuations. Eventually, the fraction of scintillation lights arrived at the photocathode surface (*i.e.*, the light collection efficiency) for every interaction points is calculated by taking average on the final weights of individual optical photons. The scintillator response is calculated by multiplying the light collection efficiency to the generated light. Since, the gamma-rays may undergo several deposition energy events, the lights obtained from various interactions in a gamma-ray history are finally summed up to calculate the simulation equivalent of detector pulse-height.

Note should be taken that the following assumptions may be made in simulation studies of scintillators: (1) It is well known that the scintillation light is produced during the interactions of charged particles with scintillator medium along their tracks. Since the secondary-electron range is very short in most applications where plastic scintillator is exposed to low-energy gamma-rays, PHOTRACK assumes that all optical photons are produced at the interaction point. (2) The scintillator response can be simply calculated through the multiplication of scintillation light, which is linearly proportional to the deposition energy [12], and the light collection efficiency. This means that the distribution of scintillation light (dN/dL) produced in the plastic scintillator when exposed to gamma-rays is similar to the deposition energy distribution (dN/dE), except in an energy-to-light conversion coefficient. One may expect that the whole light spectrum moves to lower amplitudes, where the horizontal axis should be simply calibrated with measurement data to obtain the final response. The light values are represented in MeVee, or MeV electron equivalent, which is a scintillation light that is produced when an electron deposit 1 MeV of its kinetic energy within the scintillator cell.

The light transport code, PHOTRACK, was first introduced in 2004 for the optical photon modeling in cylindrical scintillators with and without lightguide [1]. The simulation results of PHOTRACK code have been verified by many experimental and simulation data of cylindrical scintillators in the last 15 years, as summarized in the following: Light transport simulations [1], scintillator timing aspects [13], MCNPX-PHOTRACK [14] and spectroscopic aspects [15].

The rectangular geometries were also developed in recent version of PHOTRACK code which is necessary for proposed imaging system simulations, where the light-boundary contact points, in a more complicated algorithm compared to the cylindrical case, are determined through intersecting the optical photon lines and six different scintillator/lightguide faces.

#### *2.2.1. Electron escape from scintillator or wall effect*

Since the ranges of secondary electrons are relatively small when the scintillator is exposed to low-energy gamma-rays, it is generally assumed that the gamma-rays deposit their whole energy losses at the interaction sites. However, this assumption is not applicable when either energetic electrons are produced or the interaction site is near to the scintillator surface, where part of the energy may be undeposited within the scintillator.

Basically, the scintillation light production, and consequently, the detector response may be altered if this so-called wall effect is not considered. Clearly, larger gamma-ray energies result in fast secondary electrons which increases the surface escape probability. As seen in Fig. 2, the influence of wall effect on deposition energy distribution is illustrated for two different incident gamma-ray energies. The effect is enhanced with increasing gamma-ray energies from 0.662 MeV (Fig. 2(a)) to 2.22 MeV (Fig. 2(b)). As one may expect, switching off the electron transport, or equivalently, ignoring the wall effect is not negligible for gamma-rays of higher energies (Fig. 2(b)).

It has been decided to run MCNPX code with PTRAC card in Type P E (*i.e.*, photon-electron tracking and deposition information) in order to investigate the wall effect. Now, in addition to the information regarding the interaction coordinates and energy transferred to the electrons at these points, the electron energy that is taken outside the boundaries can also be calculated. Therefore, one may consider the wall effect by subtracting this energy from the energy deposited at the interaction site. Another advantage of tracking the secondary electrons is that it takes into account the energy deposition events in which

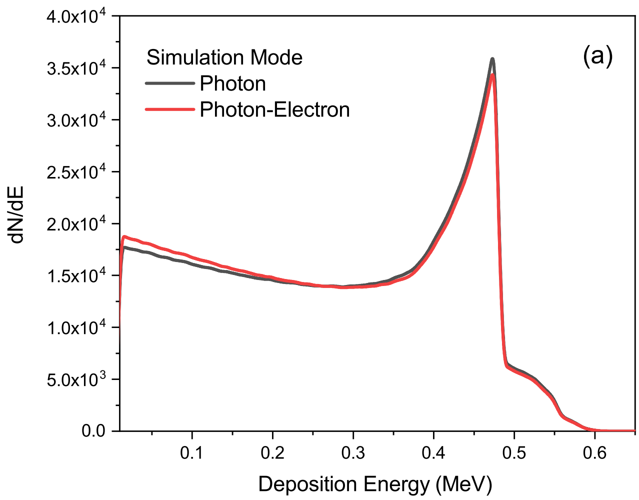


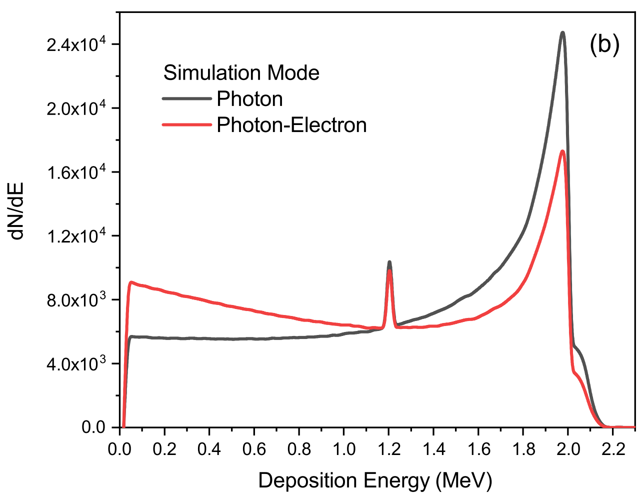


**Fig. 2.** Deposition energy spectra calculated with MCNPX code for a 2 × 2 × 20 cm$^3$ NE102 scintillator when the lateral surface is exposed to (a) 0.662 MeV and (b) 2.22 MeV gamma-rays, with and without electron transport. The peak around 1.2 MeV corresponds to gamma-ray double-escape events.

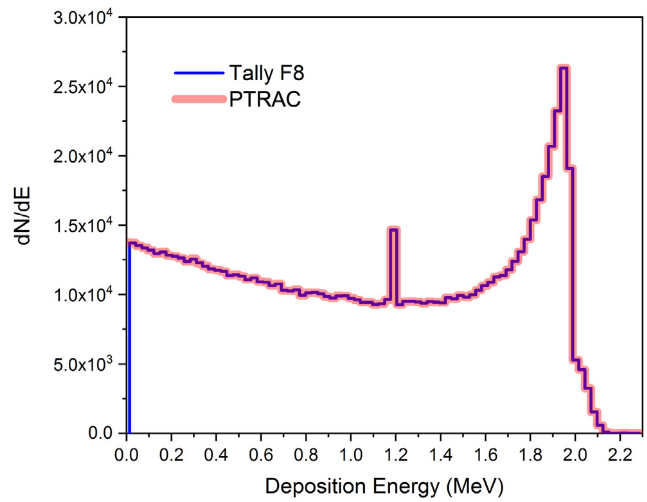


**Fig. 3.** Deposition energy spectra calculated from both PTRAC output file and F8 tally for a 2 × 2 × 20 cm$^3$ NE102 scintillator when exposed to 2.22 MeV gamma-rays.

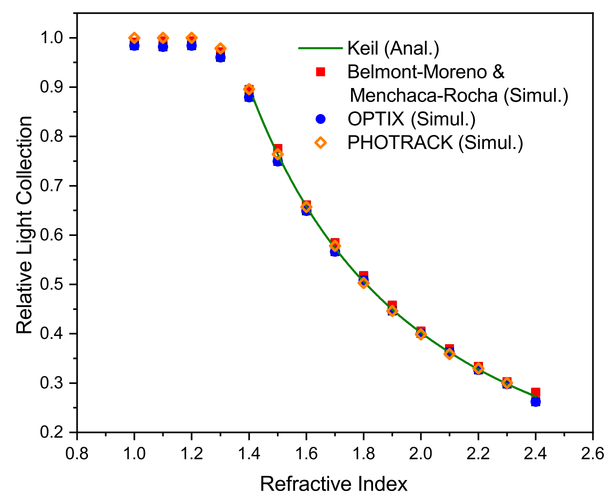


**Fig. 4.** Comparison on relative light collections calculated for a symmetric rectangular scintillator versus the refractive index for PHOTRACK, OPTIX [16], Keil [17] and Belmont-Moreno and Menchaca-Rocha [18] data.

the gamma-rays interact with the surrounding materials before the resulting electrons enter the scintillator cell. The PTRAC output usually becomes a huge and rather complicated file due to the numerous and successive electron collisions, which requires a precise reader/post-processing program. Having developed a new reader program, the deposition energy spectrum for a plastic scintillator when exposed to 2.22 MeV gamma-rays has been calculated from the PTRAC output file (Fig. 3).

#### 2.2.2. *Verification of PHOTRACK code for rectangular geometry*

In order to verify the PHOTRACK code in rectangular geometries, the studies undertaken by Safari et al. [16] were chosen, where the simulation results of OPTIX code were compared with both the semi-analytical formula of Keil [17] and also the simulation performed by Belmont-Moreno and Menchaca-Rocha [18]. In their studies, the optical photons were homogeneously produced in a 1 cm$^3$ symmetric rectangular scintillator in which light attenuation was ignored. As shown in Fig. 4, the relative light collection was plotted versus the scintillator refractive index. The comparison exhibits that PHOTRACK and all three sets of data are in excellent agreement, which confirmed the precision of tracking algorithm in rectangular geometry implemented in PHOTRACK.

In another investigation, the measurements were carried out with 4.16 × 4.16 × 5.47 cm$^3$ rectangular NE102 plastic scintillator with two surface types (*i.e.*, polished and teflon-wrapped (well equivalent to painted surface)), attached to an XP2020 PHOTONIS photomultiplier tube (PMT) and surrounded by a light-tight aluminum housing. The measurements were performed with 1 $\mu$Ci $^{137}$Cs gamma-ray source.

The detector responses calculated with MCNPX-PHOTRACK hybrid code and convoluted with a Gaussian broadening function to include the PMT contribution are compared with corresponding measured data (Fig. 5(a) and (b)), when the scintillator surface is either polished or painted (or equivalently, teflon-wrapped), respectively.

### 2.3. *Light transport simulation with FLUKA*

The general-purpose code, FLUKA, is capable to perform the generation and transport of optical photons. This feature together with ionizing radiation transport capability can be used in a full-simulation of detector response. Therefore, unlike simulations with dedicated light

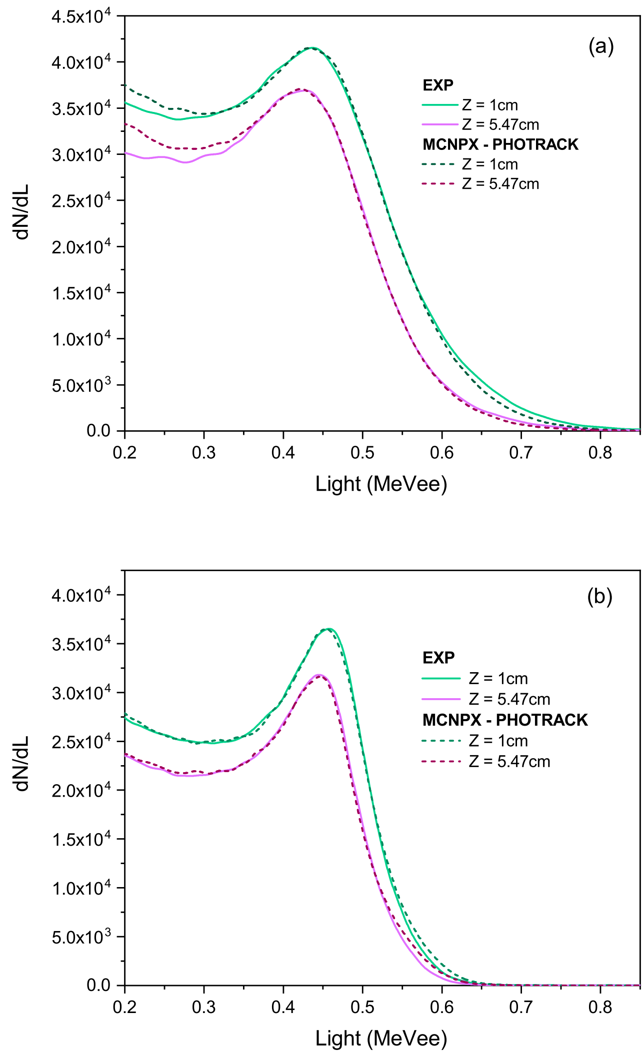


**Fig. 5.** Pulse height spectra simulated with MCNPX-PHOTRACK hybrid code and the corresponding experimental data for a plastic scintillator exposed to $^{137}$Cs gamma source when the surface is (a) polished and (b) painted (Z represents the longitudinal distance from the PMT).

transport codes such as PHOTRACK and OPTIX, which require deposition energy information as input data, FLUKA has an advantage to provide the user with a complete radio-optical simulation package.

In FLUKA, the optical photons are introduced by enabling OPT-PROD and OPT-PROP cards in FLUKA user graphical interface called flair. Several user-routines related to optical photons can also be utilized to define optical features in a more flexible details. The optical photon production in specified materials is activated by OPT-PROD card and it can be adjusted in terms of wavelength, frequency or energy. Another pre-set data in OPT-PROD card is fraction which is a portion of deposition energy that is converted into light which has to be determined by experimental light yield values. Having assumed that all scintillation photons are produced with the same wavelength, and according to the definition of light yield which is the number of optical photons per 1 MeV deposition energy, the fraction can be calculated via the relation, fraction = light yield (photons/MeV)×optical photon energy (MeV).

The optical properties of the materials that contribute to the light transport problem (*i.e.*, refractive index, absorption and diffusion coefficients), the corresponding wavelength-dependencies and also the surface boundary conditions are defined by the user either in OPT-PROP card or in related user-routines.

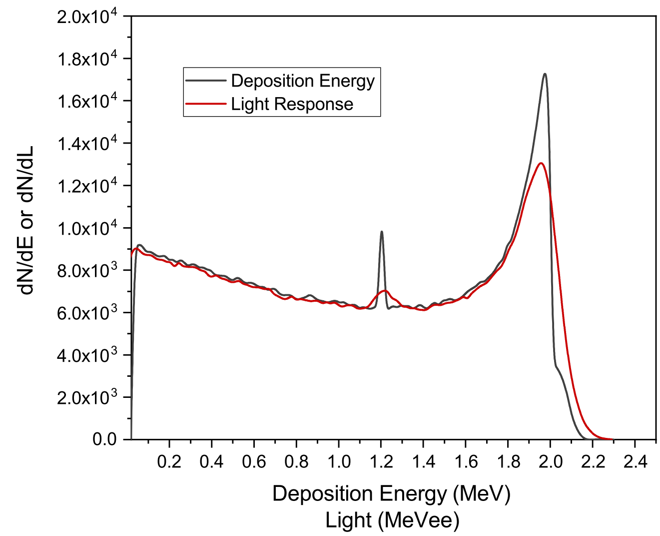


**Fig. 6.** Deposition energy versus light distributions for a 2 × 2 × 20 cm$^3$ NE102 scintillator.

Finally, the detector response or the distribution of frequency counts taken over the optical photon energies of all those crossing the PMT window for every primary gamma-ray is calculated.

## 3. Results and discussion

### 3.1. Light-transport incorporated response

Having undertaken several corrections and necessary modifications, the final rectangular-geometry version of PHOTRACK code has been successfully developed for the light transport simulations. Fig. 6 shows the simulated detector response when it is exposed to a beam of 2.22 MeV gamma-rays, before and after incorporating the light transport simulation. The response without the light transport simulation is the deposition energy distribution in the scintillator sensitive volume that was calculated by tally F8 (*i.e.*, pulse-height tally) of the MCNPX code. The incorporation of light transport simulation has significant effects on the detector response which can be specifically summarized as moving the pulse-heights to lower amplitudes and a Gaussian broadening. These effects are due to the loss of optical photons during the transport and also the statistical nature of the process.

The use of the FLUKA code in calculating the scintillator response in similar conditions resulted in a fairly identical response to the MCNPX-PHOTRACK code, as shown in Fig. 7.

### 3.2. Uniformity of scintillator response

The measurement setup in thermal neutron imaging system is such that each scintillator is longitudinally irradiated with 2.22 MeV gamma-rays. In the preliminary simulations [10], the deposition energy distribution was considered as the scintillator response, which was uniform for different longitudinal irradiations (Fig. 8). The light transport incorporation to the scintillator response will alter the response uniformity, such that the simulated scintillator response is completely different for various irradiated heights (Fig. 9).

As discussed earlier, the appropriate thermal neutron image in the proposed system requires all scintillators to have uniform longitudinal response. Since this uniformity corresponds to less diverse optical photon histories, it generally results in an improved detection resolution.

In this study, it has been decided to use the well known removal technique where in a fully painted scintillator, the light escape probability near the PMT is gradually increased by removing the reflective

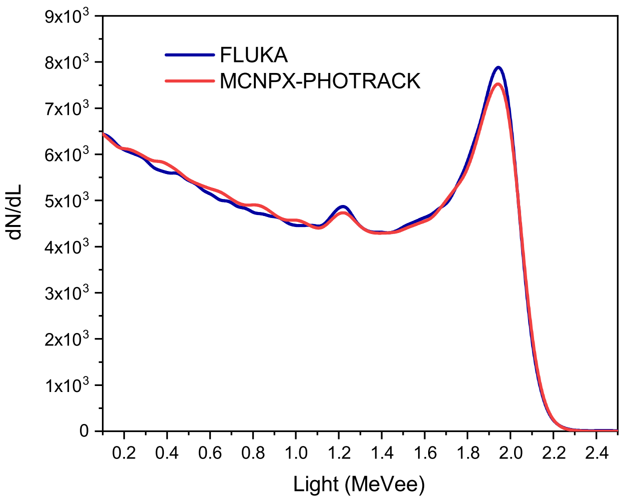


**Fig. 7.** Simulated response of a 2 × 2 × 20 cm³ NE102 scintillator exposed to an isotropic 2.22 MeV gamma ray source calculated with MCNPX-PHOTRACK hybrid code and FLUKA.

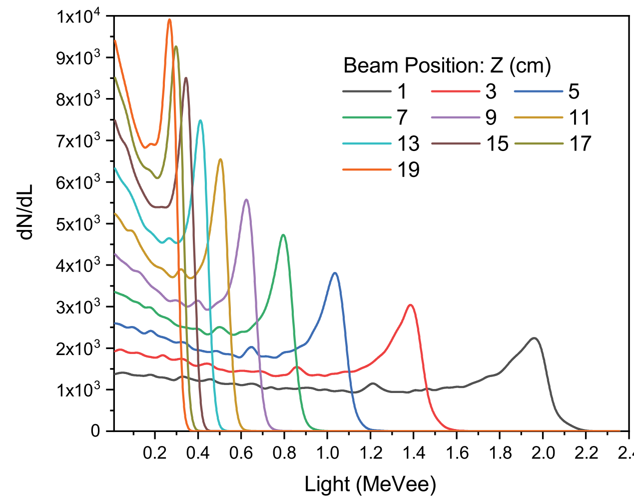


**Fig. 9.** Simulated light response spectra of a 2 × 2 × 20 cm³ fully-painted NE102 scintillator when irradiated with 2.22 MeV gamma-ray beam at different lateral heights (Z represents the longitudinal distance from the PMT).

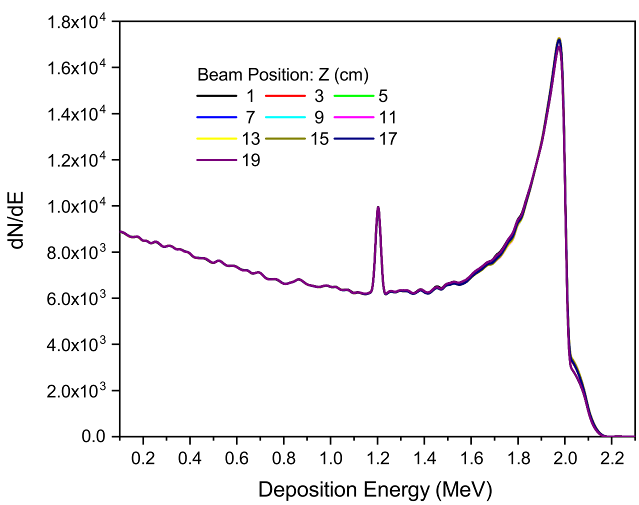


**Fig. 8.** Deposition energy spectra of a simulated 2 × 2 × 20 cm³ NE102 scintillator when irradiated with 2.22 MeV gamma-ray beam at different lateral heights (Z represents the longitudinal distance from the PMT).

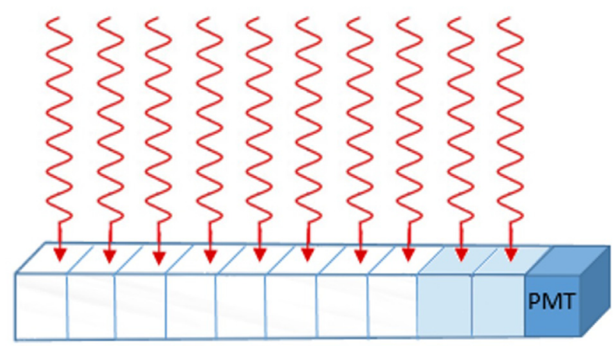


**Fig. 10.** The sketch of a long rectangular scintillator (20% of reflective paint is removed at the PMT window located at Z = 0) and different irradiation conditions.

paint near the PMT window. This causes the scintillator response when irradiated near the PMT end becomes more similar to the responses far from it.

Following the above removal technique, it was decided to remove 1 cm of paint at each stage, starting from fully pained up to fully polished surface, when the irradiation of 20-cm length scintillator by a beam of 2.22 MeV gamma-rays was simulated. Therefore, there would be 21 different surface- and 10 irradiation conditions, as shown in Fig. 10.

Since the organic scintillators do not represent photopeak in their spectra, the Compton edge energy is generally considered as a good measure to compare the scintillator responses in different irradiation conditions for each surface covering.

The 2D and 3D illustrations of Compton edge for the light-transport-incorporated simulated response of plastic scintillator as a function of both irradiation point and unpainted surface percentage is plotted in Fig. 11(a) and (b), respectively. The maximum uniformity of Compton edge is seen for larger polished (*i.e.*, unpainted) percentages.

In another comparison, the relative standard deviations of Compton edges simulated for different longitudinal irradiation heights have been calculated for different polished percentages and plotted in Fig. 12. The data confirms that when the scintillator surface is fully polished, the least diversity of Compton edge values is achieved which is corresponding to the best available detection resolution and longitudinal uniformity.

The responses of the fully-polished NE102 plastic scintillator when exposed to 2.22 MeV gamma-rays have been modeled in a set of separate simulations with MCNPX-PHOTRACK and FLUKA codes. As it can be seen in Fig. 13(a) and (b), both MCNPX-PHOTRACK and FLUKA codes agree that in fully-polished case, the scintillator response for a large portion of scintillator length remains uniform, except the region very near to the PMT window (*i.e.*, Z = 1 cm in Fig. 13(a) and (b)).

The important conclusion that can be drawn is that if plastic scintillators of 2 cm longer lengths are used in thermal neutron imaging

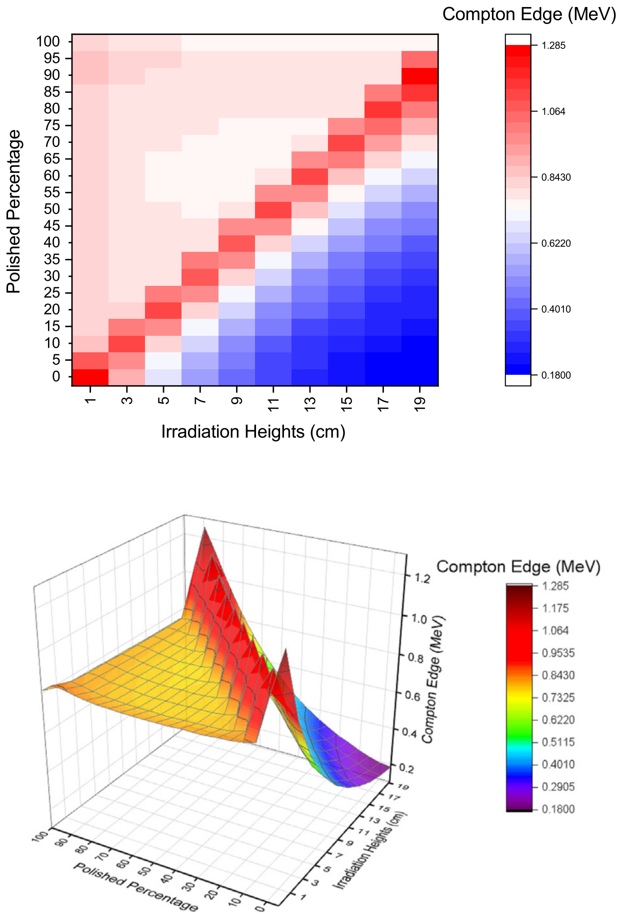


**Fig. 11.** A (a) 2D, and (b) 3D illustrations of Compton edge energy versus the irradiation heights and polished percentages. In these simulations the 2 × 2 × 20 cm$^3$ NE102 scintillator is irradiated with 2.22 MeV gamma-ray beam.

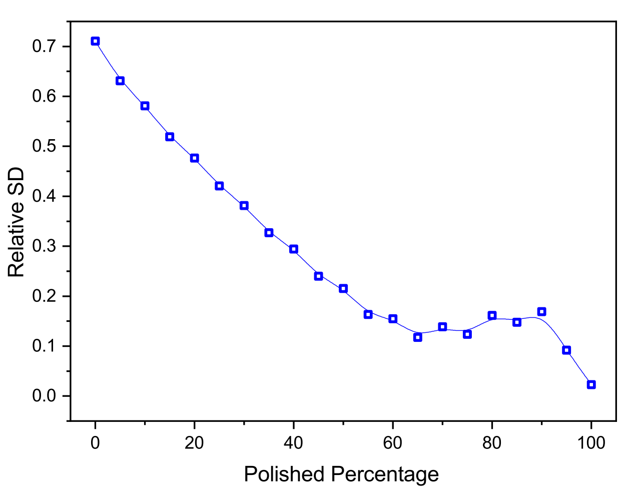


**Fig. 12.** Relative standard deviation of Compton edge energy simulated for ten irradiation heights in different polished percentage (from 0 to 100) of scintillator surfaces.

system, one may expect that all 17 scintillators exhibit uniform longitudinal responses when exposed to collimated beams of gamma-ray incident from the water phantom.

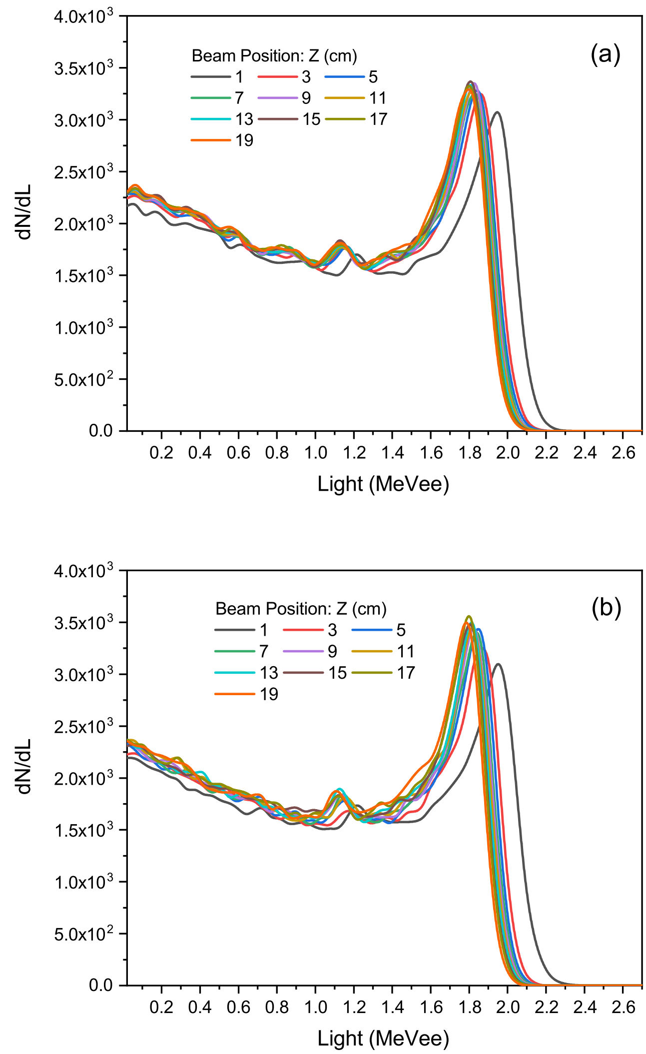


**Fig. 13.** (a) MCNPX-PHOTRACK and (b) FLUKA simulated response functions for the best longitudinal uniformity obtained in the fully polished situation (Z represents the longitudinal distance from the PMT).

To this purpose, two plastic scintillators have been chosen, one from ten vertical- and one from seven horizontal detectors of the imaging system, however, all lengths are 2 cm larger at the PMT side. As it can be seen in Fig. 14(a) and (b), an excellent longitudinal uniformity exists among the two selected sets of scintillators.

## 4. Conclusions

The conceptual design of a thermal neutron imaging system consisting of 17 long plastic scintillators was introduced in [10]. A more accurate and comprehensive simulation of the detection setup requires the optical photon in addition to ionizing radiation transport. A common problem associated with large and/or long scintillators is that their responses are highly dependent on the irradiation location due to large light losses that usually occur during several attenuations inside the scintillator volume and reflections at the boundaries. In order to resolve this problem, a paint removal technique was proposed. The result confirmed that in fully-polished scintillator case, the detector response to gamma-rays incident on entire lateral area, except near the PMT window, is almost uniform, resulting in an optimum pulse-height resolution, which is in line with previously published works [19,20]. It was anticipated that all 17 scintillators could exhibit uniform longitudinal responses when exposed to collimated gamma-rays incident from

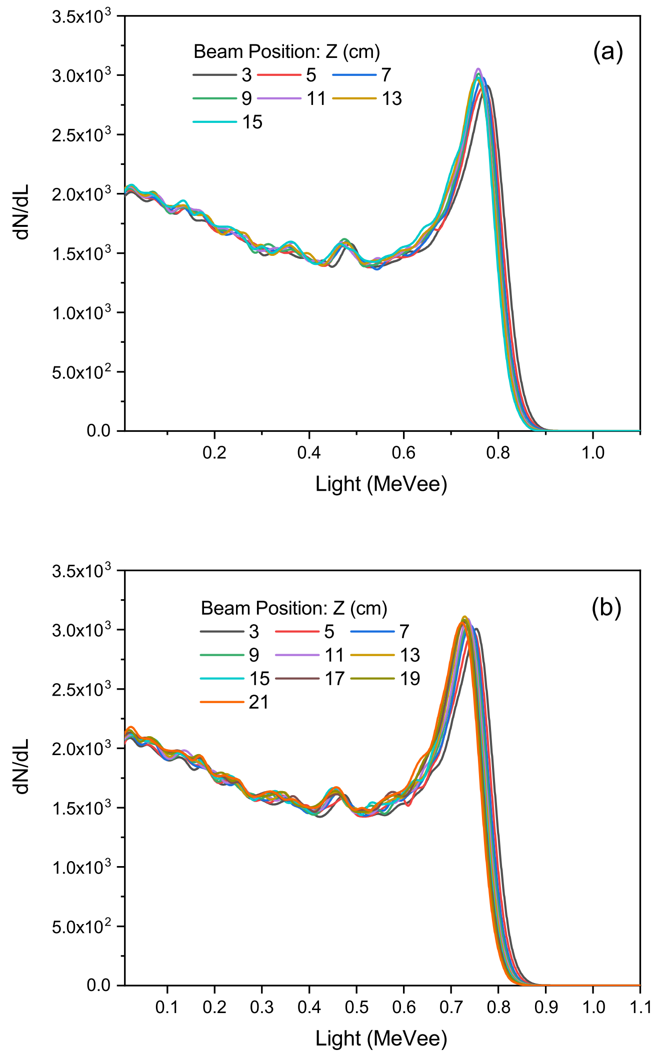


**Fig. 14.** Simulated responses of (a) 2 × 2 × 16 $cm^3$ and (b) 2 × 2 × 22 $cm^3$ NE102 scintillators when longitudinally irradiated with mono-energetic gamma rays. The detection setup is such that the first 2 cm of scintillators lengths from PMT end are left unirradiated (Z represents the longitudinal distance from the PMT).

the water phantom if scintillators of about 2 cm longer length from the PMT end are used.

## Acknowledgments

We would like to thank the reviewers for careful reading the manuscript and their very thoughtful comments.

## References

[1] N. Ghal-Eh, M.C. Scott, R. Koohi-Fayegh, M.F. Rahimi, A photon transport model code for use in scintillation detectors, Nucl. Instrum. Methods Phys. Res. A 516 (2004) 116–121.
[2] J. Tickner, G. Roach, PHOTON-An Optical Monte Carlo code for simulating scintillation detector responses, Nucl. Instrum. Methods Phys. Res. B 263 (2007) 149–155.
[3] A. Ferrari, P.R. Sala, A. Fasso, J. Ranft, FLUKA: A Multi-Particle Transport Code (Program Version 2005) (No. INFN-TC-05-11), 2005.
[4] GEANT4 Collaboration, GEANT4-a Simulation toolkit, Nucl. Instrum. Methods Phys. Res. A 506 (2003) 250–303.
[5] R.G. Peyvandi, A. Taheri, A. Olfateh, S.Z. Islami, A new automated and precise calibration method for gamma level gauges with rod detector arrangement, Appl. Radiat. Isot. 112 (2016) 1–4.
[6] A. Blondel, et al., A fully-active fine-grained detector with three readout views, J. Instrum. 13 (2018) P02006.
[7] M. Taiuti, et al., Measurement of the response of long plastic scintillator bars for the large angle electromagnetic shower calorimeter for CLAS, Nucl. Instrum. Methods Phys. Res. A 370 (1996) 429–434.
[8] J.S. Hendricks, et al., MCNPX 2.6.0 Extensions, Los Alamos National Laboratory, 2008.
[9] S. Green, Estimation of tritium production in fusion blankets (Ph.D. thesis), The University of Birmingham, UK, 1988.
[10] N. Ghal-Eh, S. Green, A plastic scintillator-based 2d thermal neutron mapping system for use in BNCT studies, Appl. Radiat. Isot. 112 (2016) 31–37.
[11] N. Ghal-Eh, R. Koohi-Fayegh, Light collection behaviour of scintillators with different surface coverings, Radiat. Meas. 41 (2006) 289–294.
[12] G.F. Knoll, Radiation Detection and Measurement, John Wiley and Sons, 2010.
[13] Z.B. Bash, N. Ghal-Eh, E. Bayat, G.R. Etaati, Lightguide influence on timing response of scintillation detectors, Radiat. Phys. Chem. 82 (2013) 1–6.
[14] M. Tajik, N. Ghal-Eh, Comparison of light transport-incorporated MCNPX and FLUKA codes in generating organic scintillators responses to neutrons and gamma rays, Nucl. Instrum. Methods Phys. Res. A 791 (2015) 65–68.
[15] M. Mottaghian, R. Koohi-Fayegh, N. Ghal-Eh, G.R. Etaati, Photocathode non-uniformity contribution to the energy resolution of scintillators, Radiat. Prot. Dosim. 140 (2012) 16–24.
[16] M.J. Safari, H. Afarideh, N. Ghal-Eh, F.A. Davani, Optix: A Monte Carlo scintillation light transport code, Nucl. Instrum. Methods Phys. Res. A 737 (2014) 101–106.
[17] G. Keil, Design principles of fluorescence radiation converters, Nucl. Instrum. Methods 89 (1970) 111–123.
[18] E. Belmont-Moreno, A. Menchaca-Rocha, Geometrical effects in charged particle detection using scintillation counters, J. Phys. D: Appl. Phys. 28 (1995) 835.
[19] J. Chen, R. Mao, L. Zhang, R.-Y. Zhu, Large size LSO and LYSO crystals for future high energy physics experiments, IEEE Trans. Nucl. Sci. 54 (2007) 718–724.
[20] Y. Xiaoguang, A study of light collection efficiency in scintillation detectors, Nucl. Instrum. Methods Phys. Res. A 228 (1984) 101–104.